Water Dissociation and Hydroxyl Formation on Ni(110)

Nikki Gerrard, Kallum Mistry, George R. Darling and Andrew Hodgson*

Surface Science Research Centre and Department of Chemistry, University of Liverpool, Liverpool L69 3BX, UK

* ahodgson@liverpool.ac.uk

Abstract

Nickel is an active catalyst for hydrogenation and reforming reactions, with reaction showing a strong dependence on the surface exposed. Here we describe the mixed hydroxyl-water phases formed during water dissociation on Ni(110) using STM and low current LEED. Water dissociation starts between 150 and 180 K as the H-bond structure evolves from linear 1D chains of intact water into a 2D network containing short rows of face sharing hexagonal rings. As further water desorbs the hexagonal rows adopt a local (2 x 3) arrangement, forming small, disordered domains separated by strain relief features. Decomposition of this phase occurs near 220 K to form linear 1D structures, consisting of flat, zigzag water chains, with each water stabilised by donating one H to hydroxyl to form a branched chain structure. The OH-H_2O chains repel each other, with the saturation layer ordering into a (2 0, 1 4) structure that decomposes to OH near 245 K as further water desorbs. The structure of the mixed OH/H_2O phases are discussed and contrasted with those found on the related Cu(110) surface, with the differences attributed to strain in the 2D H-bond network caused by the short Ni lattice spacing and strong bond to OH/H_2O.

Introduction

Along with copper, nickel is an important catalyst in re-forming reactions [1-3], finding application in practical catalysts for water dissociation and re-forming [4-5]. The reactivity of both metals is extremely face dependent, with water remaining intact on the close packed faces [6-8] but dissociating at moderate temperatures on more open surfaces [9-10] as the water binding energy increases [4-5, 11-13]. The open (110) surface is the most widely studied reactive face, with early reports suggesting copper and nickel form similar water structures [14-16]. However, the two metals differ considerably in their reactivity and lattice spacing, and more recent studies indicate significant differences between their interaction with water. For example, water adsorbs and desorbs below room temperature on Cu(110) without dissociating [17], forming 1D chains of face sharing pentamers that aggregate into a 2D network only at high coverage [18]. The behaviour on Ni(110), where water has a higher binding energy, is quite different. Instead of forming cyclic, face-sharing water rings, water instead forms linear, two-coordinate zigzag chains along the

close packed Ni rows, maximising bonding to Ni at the expense of a reduced H-bond coordination [19].

The high binding energy of water to nickel is also reflected in the greater reactivity of this surface. Cu(110) surfaces dissociate water only when it is adsorbed above 255 K [10], but hydroxyl can also be formed by reaction with pre-adsorbed O atoms at low temperature [14, 20-21]. By using the O surface reaction to form known amounts of hydroxyl, three different partially dissociated phases can be characterised on Cu(110). A ($2H_2O$+1OH) c(2x2) structure forms at low temperature, consisting of a distorted, 2D hexagonal network containing OH Bjerrum defects [22]. This structure decomposes on heating to form a ($1H_2O$+1OH) structure, containing 1D water chains decorated by OH, and then a pure OH phase that finally decomposes to O and water [22]. In contrast, water dissociates spontaneously on Ni(110) before it desorbs [9, 23], although there has been disagreement over both the onset temperature and degree of dissociation [9, 15-16, 24-32]. Although the reaction of O with water is stoichiometric at low coverage and temperature, Guo and Zaera showed that additional water dissociates to form OH and H, so this reaction cannot easily be used to prepare known OH/H_2O ratios on Ni(110) [23]. Thermal desorption spectra of water from Ni(110) (Fig. 1) are similar to those obtained for H_2O/OH on Cu(110), with three desorption peaks appearing at temperatures above the water multilayer peak [9, 23, 29]. The high temperature peak is due to OH disproportionation to form O and water [16, 23-24], similar to Cu(110) [33], but it is not known if the two lower temperature desorption features correspond to the same structures as form on Cu, or are different. Moreover, thermal desorption spectra following water reaction with O on Ni(110) show differences from pure water adsorption [23], where the hydrogen formed by dissociation only desorbs from the surface above 250 K [34] and can itself reconstruct the surface [35], so the nature of the hydroxyl structures formed on Ni(110) remains unclear. Since hydroxyl is a key species in the catalytic surface redox chemistry of many small molecules [36], including on Ni [37-39], understanding the different water oxidation states on this surface remains an important goal [40-41].

In this study we explore the dissociation of a water film on Ni(110) using low temperature STM. Thermal desorption spectroscopy (TDS) is combined with low current LEED to determine the lateral order of the different structures formed without influence from electron induced restructuring [42], allowing us to relate the STM measurements to previous experimental studies [9, 15-16, 24-32]. We find that above 150 K dissociation occurs in parallel with water desorption to form first a disordered 2D water/hydroxyl network, with a variable OH/H_2O composition, then an ordered array of 1D (OH+H_2O) chains. We contrast the reactivity of the open Ni and Cu surfaces and discuss how the short Ni lattice spacing influences the structures formed on Ni.

Methods

The Ni(110) surface (Surface Preparation Laboratory) was cleaned by Ar^+ ion sputtering and annealing to 950 K. Water adsorption was characterized in two separate chambers. LEED and temperature programmed desorption measurements were carried out in a chamber equipped with a calibrated molecular beam to dose known amounts of water onto the surface. The water flux was calibrated against the ordered monolayer structure formed on Cu(511) [43], allowing the surface coverage to be chosen to ±2% monolayer. Thermal desorption spectra were recorded as a function of initial coverage and heating rate using a VG Micromass quadrupole mass spectrometer. Surface ordering was determined using a low current, dual micro-channel plate LEED system (OCI) operated at currents of less than 1 nA to avoid electron induced dissociation or restructuring of water. STM measurements were carried out using a Createc STM with the sample held at 80 K during adsorption and imaging, prior to annealing to different temperatures [43]. Images were recorded in constant current mode with an electrochemically etched tungsten tip. STM images of water were essentially insensitive to the tip bias conditions between ±0.5 V and I<250 pA, and were processed using WSXM [44].

Results

Depositing water on to Ni(110) and heating the surface to induce dissociation or desorption gives rise to the water thermal desorption profiles shown in Figure 1. The spectra are similar to those reported previously [16, 27], with a low temperature peak (C) near 155 K, associated with multilayer water desorption, and three higher temperature peaks at 215 K (A2), 245 K (A1) and 355 K (B). Water desorption peaks appear at very similar temperatures for H_2O and D_2O, but the shape of the A2 peak is noticeable different between the two isotopes, being slightly broader for D_2O, while at low coverage the A1 peak is smaller for D_2O than for H_2O. Although the A1 and A2 peaks do not shift with coverage, suggesting they are approximately zero order, it is not possible to describe them by any simple kinetic scheme or extract an activation barrier for water desorption. A leading edge analysis of the A2 peak finds an apparent activation energy for H_2O desorption that increases from ca. 52 to 120 kJ mol^{-1} as the coverage is increased from 0.25 ML to ≥1 ML, reflecting the complex dissociation/desorption kinetics that lead to formation of the A2 phase in which water is stabilised by H-bonding to OH. The increasing apparent activation barrier is consistent with the idea that water is stabilised at higher coverage and temperature as the amount of OH present increases [31]. As has been noted previously, the desorption profile of water from Ni(110) is very similar to the three peaks formed by reaction of O and water on Cu(110), but the corresponding peaks on Ni(110) lie 25 to 75 K higher than on Cu(110), indicating a higher binding energy on Ni [45].

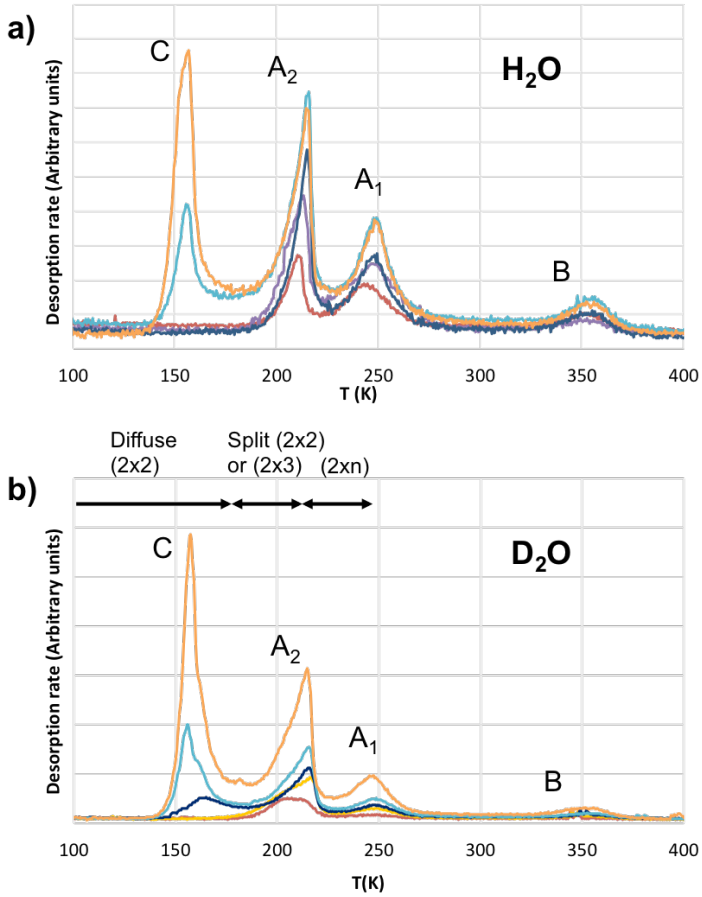

Figure 1. Water thermal desorption spectra recorded for different initial coverage of a) H_2O and b) D_2O, adsorbed onto the Ni(110) surface at 100 K and heated at a rate of 2 K s^{-1}. The peaks are labeled as previously reported [29] and the initial coverage is approximately 0.5, 1, 1.5 and 2 ML for H_2O and 0.5, 1, 1.5 and 3 ML for D_2O. The LEED pattern for both isotopes is similar and is indicated schematically between the spectra.

Ordering of the surface structures during water dissociation was determined by recording the LEED pattern during thermal desorption and is summarized in Fig. 1, with further detail given in the Supplementary Information. The intact phase formed at 100 K consists of domains of flat zigzag water chains in a (2 x 2) or (4 x 4) arrangement below 0.5 ML, with water decorating the remaining exposed Ni rows as the coverage is increased further to form a disordered monolayer, with a diffuse (2 x 2) LEED pattern and faint ¼ order features [19]. Heating the surface above 150 K to initiate dissociation and desorb excess water causes the half order LEED beams to split along the $[001]$ direction towards a (2 x 3) repeat. As water starts to desorb in the A2 feature, additional splitting appears corresponding to a length scale of *ca.* 6 to 7 times the Ni repeat along $[1\bar{1}0]$. Finally, as the A2 peak completes and the A1 phase is formed, the

LEED pattern streaks along [001] and a (2 x n) structure appears, where n depends on the initial water coverage. Desorption from a fully saturated water surface (coverage ≥ 1 ML) results in a sharp, well-defined (2 0, 1 4) LEED pattern appearing for the A1 phase. Previous conventional LEED studies of water on Ni(110) may have been compromised by electron induced dissociation and have usually focused on the diffuse c(2 x 2) structure, although other structures have also been reported, including (2 x 1), c(2 x 4) and c(2 x 6) structures [16, 27, 46]. The LEED patterns described above can be directly related to STM images of the partially dissociated OH/H_2O structures formed as water desorbs in the A2 and A1 peaks, as discussed below.

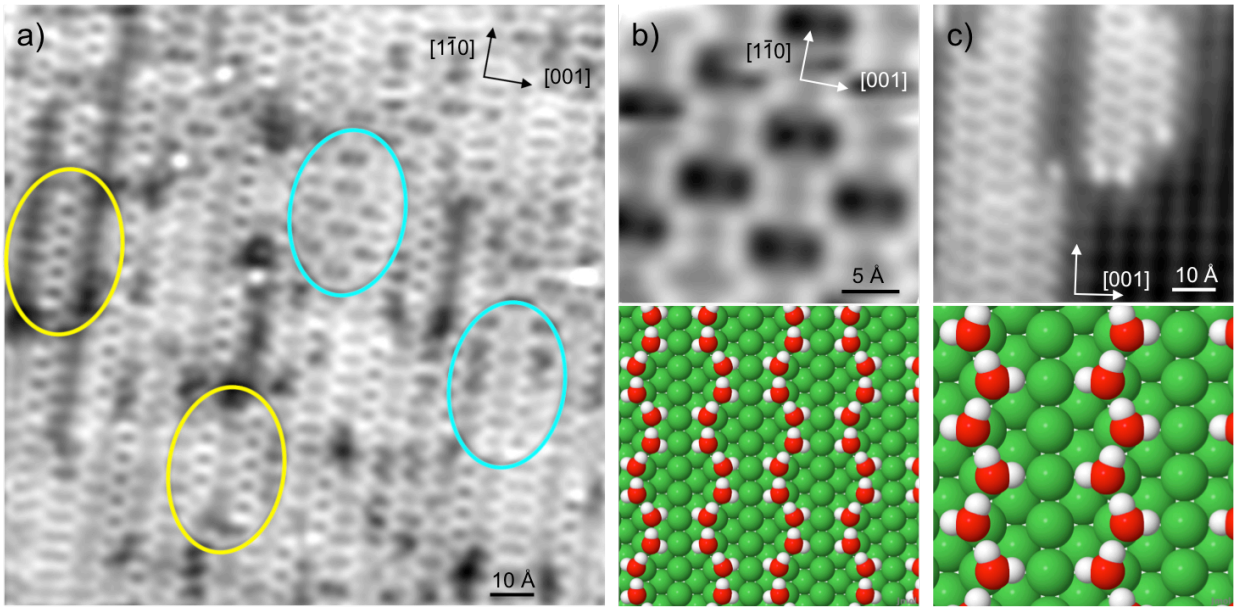

Figure 2. a) STM image showing the structures formed after water is heated to 183 K, just prior to water desorption in peak A2 (Fig. 1), and then cooled to 80 K. The regions marked blue highlight local structures corresponding to (b) a (4 0, 2 2) structure and (c) a (2 0, 1 2) repeat that is observed for intact water at a coverage of 0.5 ML at 80 K. In addition to these intact water structures, image (a) also contains short chains of face sharing hexamers, examples of which are highlighted in yellow and discussed in the text. Frames b) & c) adapted from *J. Phys. Chem. Lett.* **2020,** *11*, 2121-2126. Image conditions a) 183 K, 265 pA, -0.30 V, b) 80 K, 240 pA, -0.38 V and c) 80 K, 175 pA, -0.09 V.

Figure 2 shows an STM image of the structures formed after the water covered surface is annealed to 183 K, just below the temperature where water desorbs in the A2 peak (Fig. 1). Note that heating in the STM occurs on a longer timescale than thermal desorption, *ca.* 1 K min^{-1} in the STM compared to 2 K s^{-1} for Fig. 2, so for a particular anneal temperature, decomposition and desorption will be more advanced in the STM images than in the

corresponding thermal desorption spectrum. The surface is covered by low contrast (*ca.* 20 pm) water structures that display local order but remain disordered on a 10s of Å scale. The structures seen in Fig. 2a can be broken down into two categories depending whether they are observed when water is adsorbed intact [19] or if they are unique to the annealed surface. Examples of features corresponding to intact water structures are highlighted in blue in Fig. 2a, and their structures shown in Fig. 2b & 2c. Intact water forms 1D chains along alternate close packed Ni rows, with either a 2x repeat (the zigzag chains, Fig. 2c) or a 4x repeat (the wiggly chains, Fig. 2b). The 1D chains are more stable than H-bonded 2D water networks, or structures with more than 0.5 ML water, and can align in different registries along $[001]$ [19]. While much of the surface can be attributed to a disordered mixture of the intact water chains shown in Fig. 2b,c, short rows of face sharing hexamers also appear, with two examples highlighted in yellow. Unlike the structures associated with intact water, where water decorates alternate close-packed Ni rows, these hexagonal rows have adsorbate bound on neighboring rows of Ni and appear only after annealing above 150 K. The face-sharing hexagonal rows are rarely more than 6 units long (30 Å) before a defect or different structure appears, and do not form immediately next to each other. In fact there is a strong preference for the hexagonal chains to appear 3 Ni repeats apart; an example is shown in the region highlighted at the bottom of Fig. 2a, where two of these hexagonal chains form a local (2 x 3) arrangement on Ni with fainter structure between the hexagonal chains. The (2 x 3) arrangement is consistent with the LEED splitting that appears between 150 and 210 K, prior to completion of the A2 desorption peak.

Figure 3 shows the structures that form as the surface is heated to 200 K to initiate water desorption via the A2 peak. The adsorbate forms patches of a 2D network that progressively disappears (see images 3a to 3d) as water desorbs and dissociates to form the 1D zigzag chains of the A1 structure, discussed later. The 2D islands are poorly ordered but contain rows of the same face sharing hexagonal rings that were starting to appear at 180 K (Fig. 2a). The hexagonal rows are aligned along the close packed Ni direction and usually spaced 3 lattice repeats apart along $[001]$, (see for example Fig. 3a), consistent with the (2 x 3) repeat seen in LEED. As water desorbs, and the coverage of the 2D phase decreases (Fig. 3b to 3d), the 2D structures remain rather disordered, with regular discontinuities breaking up the structure into smaller domains between every 5 or 6 rings along $[1\bar{1}0]$ and into increasingly small (2 x 3) patches along $[001]$ as desorption proceeds. The face sharing hexagonal rows are relatively well defined, often showing higher contrast features within the rows, but the structure between the hexagonal rows is faint and appears disordered. Eventually the 2D islands narrow, forming first small (2 x 3) domains spanning a width of just 4 Ni rows (highlighted by yellow ellipses, Fig.

3c, d) and then isolated rows of face sharing hexagons linked to zigzag chains (highlighted in blue, Fig. 3d). The presence of single rows of face sharing hexagonal rings in the high coverage layer as the A2 structure initially forms (Fig. 2a) and as the last cyclic structure left as the A2 phase decomposes into the zigzag chains of the A1 structure (Fig. 3d) suggests that the hexagonal rows themselves are the key structural element of the A2 structure, not the (2 x 3) paired arrangement. The structure of the A2 phase will be discussed in more detail later, once we have described the A1 structure, which is rather simpler to understand.

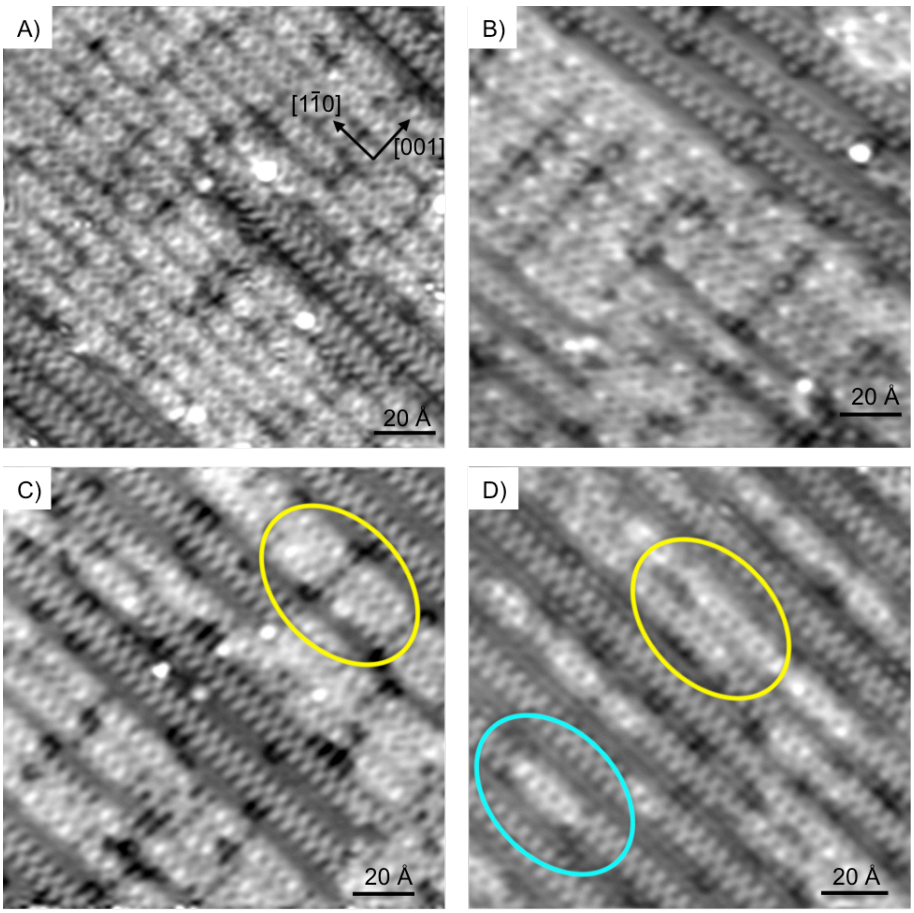

Figure 3. Water structures formed after annealing a water covered surface to 200 K and cooling to 80 K to image. Frames (a) to (d) show regions of decreasing coverage as water desorbs in the A2 peak, converting from a 2D structure into the 1D zigzag chains that make up the A1 phase. The STM images are rather insensitive to bias conditions and show a contrast of 20-25 pm for the zigzag chains and 40 pm for the bright features in the hexagonal rows (e.g. in centre of Fig. 3b). The regions highlighted are discussed in the text. Image conditions a) 175 pA, -56 mV, b) 2018 pA, -52 mV, c) 180 pA, -43 mV, d) 215 pA, -54 mV.

As water desorption proceeds slowly in the A2 peak at 200 K, the 2D structures progressively disappear to leave 1D zigzag chains that run along the close packed $[1\bar{1}0]$ direction, Fig. 3d. Annealing the surface to 220 K (Fig. 4) completely removes the remaining patches of 2D structure and the zigzag chains order into a regularly spaced array that characterizes the A1 phase. Starting from a monolayer or more of water results in an array with the chains arranged 4 Ni rows apart in an anti-phase arrangement to give the (2 0, 1 4) structure (Fig. 4b) that is observed in LEED. Lower starting coverage results in a greater spacing between the chains, (e.g. see Fig. 5a where the chains are 5 Ni rows apart), but they never appear closer than 3 Ni rows apart, indicating a predominantly repulsive interaction between the chains. The zigzag 'Z' chains have open branches that point slightly up or down the chains and are similar to the OH-H_2O chains that have previously been characterized on Cu(110), where this structure is responsible for the equivalent thermal desorption peak [33]. Water bonds in a flat, H-bonded zigzag arrangement along the close packed Ni rows, either side of the Ni atop position, Fig. 4c. The H atom that points away from the chain axis forms an H-bond to OH, bonded in the Ni bridge site, to create the characteristic branched chain arrangement. In some regions, for example at the top of Fig. 4a, small sections of the OH-H_2O chain structure sometimes arrange with water in alternating pairs along the Ni rows to form a 4x repeat, 'pinch' type structure, denoted P, see Fig. 4d. Again, this minority structure binds water near the atop site and OH in the bridge site and is similar to the P chains reported on Cu(110) [33, 47].

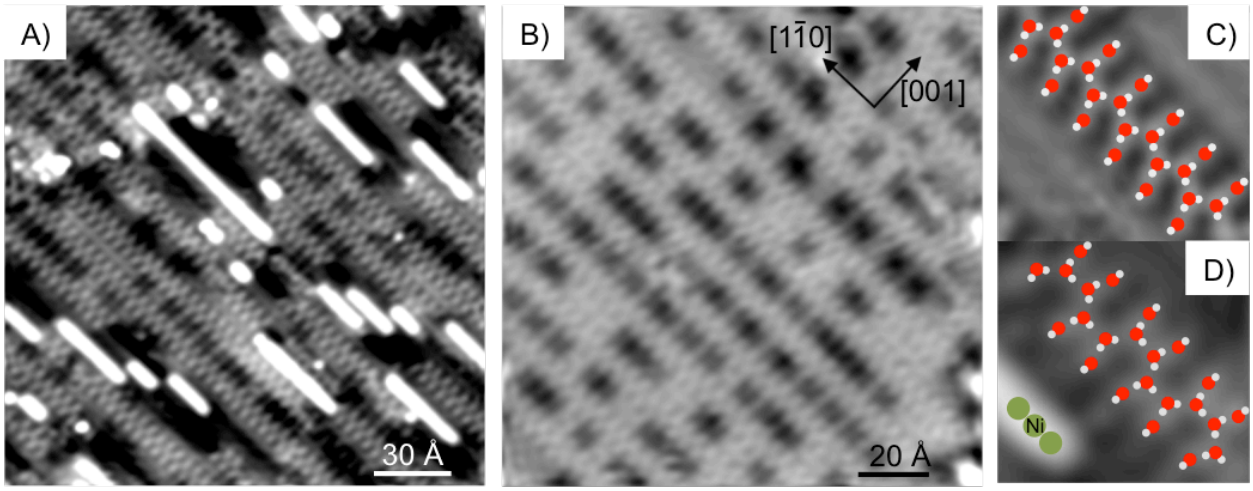

Figure 4. STM images of the A1 structure formed after annealing to 220 K to complete decomposition of the A2 structure. a) shows a low coverage region with bright (~110 pm apparent height) added rows of Ni and fainter (20 pm) OH-H_2O chains. b) a high coverage region showing the ordered zigzag OH-H_2O chains in the (2 0, 1 4) structure formed after dissociation of a water multilayer. Two slightly different arrangements of OH-H_2O chain are observed, a zigzag, 'Z' chain shown in (c) and the minority pinch, 'P' structure, shown in (d),

with a 2x or a 4x alternation of water either side of the Ni atop position and OH in the adjacent short bridge position [33]. Image conditions a, c, d) -83 mV, 190 pA and b) -65 mV, 203 pA.

Apart from the similar structure of the OH-H_2O chains formed on Ni and Cu(110), we also observe high contrast (110 pm) linear features between some Ni rows that we attribute to monatomic Ni wires, similar to those seen after water dissociation on Cu(110) [47]. The Ni wires sometimes lie alongside the OH-H_2O chains, but also next to exposed Ni patches. As for Cu(110) [47], these Ni chains do not appear on clean Ni(110) and are evidently stabilized by H adsorption, which can lead to the (1x2) missing row reconstruction on both surfaces. Some other features seen on Ni(110) have not been reported on Cu. A contrast decrease is observed in the Ni around some of the OH groups along the zigzag OH-H_2O chains as the 2D phase disappears (e.g. see the 'C' shaped dark depressions around some OH features in Fig. 3c), while Fig. 4b shows a (2 0, 1 4) ordered domain covered by OH-H_2O chains with a contrast variation of *ca.* 20 pm along the exposed Ni between the chains. Although this variation might arise from differences in the local H coverage, changing the Ni workfunction, H is mobile at 80 K and high-resolution images suggest a different explanation. Figure 5a shows the chain structure after slow annealing at 220 K to allow some decomposition of the OH-H_2O chains. Additional features appear decorating some OH groups along the side of the OH-H_2O chains, surrounded by a low contrast region. The additional features are assigned as excess OH groups, formed as the OH coverage increases beyond the 1:1 ratio of the OH-H_2O chains. On Cu(110) the pure OH phase consists of OH dimers, with one OH lying flat in the short bridge site, donating to a second OH on the next Ni row that is tilted out, away from the surface [33]. This OH dimer images as two very faint protrusions on Cu(110), surrounded by an extensive low contrast region [48], similar to the features seen at the edge of the chains in Figs. 3c, 3d and 5a. Decorating the OH groups along the edge of the OH-H_2O chain with a second OH forms an OH dimer with a similar arrangement as on Cu, but with the first flat OH H-bonded to the water chain, as indicated schematically on the STM image in Fig. 5a.

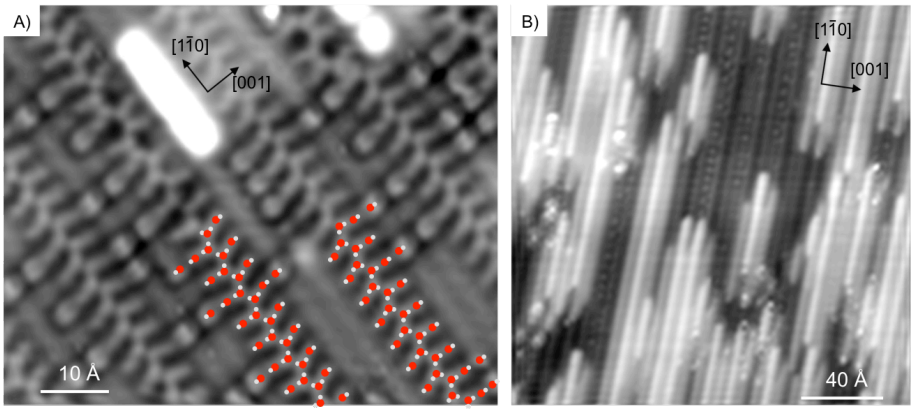

Figure 5. a) STM image after extended annealing of water to 220 K to allow partial decomposition of the OH-H_2O structure to create excess OH. A model of the structure is superimposed on two of the chains to show the additional OH groups decorating some of the chains. b) STM image following annealing to 270 K to decompose the OH-H_2O chains. Image conditions a) 185 pA, -1.0 V, b) 115 pA, -0.16 V.

Further heating causes the OH-H_2O chain structure to decompose around 245 K, as desorption peak A1, to leave just OH on the surface. Thermal desorption indicates the OH is stable up to 350 K before it disproportionates, evolving more water (Peak B, Fig. 1) to leave O on the surface [16, 23-24]. Annealing the surface to 270 K results in the surface shown in Fig. 5b. The surface is extremely corrugated, with a high density of added Ni rows, presumably stabilized by either the adsorbed OH or by H, which only desorbs the surface slowly below 300 K [34]. Isolated features appear along the Ni rows (top center Fig. 5a) with a contrast of *ca.* 15 pm, similar to that seen for OH in the low temperature phases, but the large surface corrugation makes it difficult to confirm if this is OH or establish its local structure with any confidence. Certainly the STM results do not indicate any clear structure that could be ascribed to a (2 x 1)-OH structure that has been reported following reaction between water and O [24, 46], and no ordered superstructure was found in LEED.

Discussion

While the thermal desorption spectra of water from Ni(110) are very similar to those observed for the mixed H_2O/OH structures formed on Cu(110) by the oxygen-water reaction, the present results show the 2D network formed (the A2 phase) is different from that found on Cu, mirroring the differences previously found for the intact water structures. In contrast, the A1 (OH-H_2O) structure appears identical between the two metal surfaces, consisting of H-bonded H_2O chains that zigzag along the close packed Ni sites, with the second water H atom donating to OH groups in the adjacent bridge site [33]. At 2.5 Å, the Ni-Ni spacing is some 0.3 to 0.4 Å shorter than the typical O separation in H-bonded water clusters [8], but the open nature of these 1D chains, which contain no cyclic rings, presumably allows the H-bond structure to accommodate the short Ni-Ni spacing by increasing the zigzag of the water backbone compared to Cu. Whereas both the ‘Z’ and ‘P’ type chains appear commonly on Cu(110), the vast majority of the (OH-H_2O) chains seen on Ni are the ‘Z’ form, where the water O alternates from one side of the Ni row to the other at each lattice point, allowing an O-O H-bond separation greater than the Ni nearest neighbor spacing. In contrast, placing two O atoms of water on the same side of the Ni chain (the ‘P’ form) either requires a rather short O-O separation, or more likely creates an increased angle between the H-bonds of the water chain. Further decoration of the edge OH

groups by a second OH occurs as the OH/H_2O ratio increases on Ni(110), allowing the chain structure to accommodate excess OH as water desorption proceeds, something that was not observed on Cu [33].

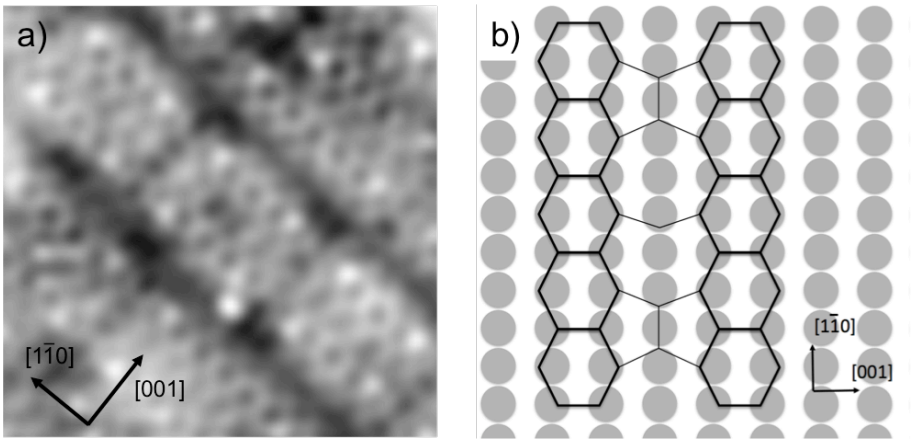

Fig. 6. a) STM image showing detail of the A2 structure prepared at 200 K. The hexagonal rows form small domains in a (2 x 3) arrangement and show several brighter features. b) schematic showing the registry of two hexagonal rows (bold hexagons) to the Ni rows. The schematic also indicates possible intermediate structure, decorating the vacant Ni row, that is chosen to be similar to the 2D domain seen in the center of a). The vertex of the lines represents an O site (OH or H_2O). Image conditions a) 190 pA, -0.09 V.

The situation for the A2 phase is very different. Whereas early measurements usually found a c(2 x 2) structure [9], or sometimes c(2 x 4) or c(2 x 6) [16, 27], the present low current LEED measurements and STM images both find a (2 x 3) overlayer, with some additional structure (LEED splitting) along $[1\bar{1}0]$. STM images show the 2D H-bond network contains short rows of face sharing hexagonal rings aligned between two close packed Ni rows, often with a (2 x 3) repeat, as illustrated in Fig. 6. This phase always remains disordered, with regular defects along $[1\bar{1}0]$ that limit the length of the hexagonal chains to at most 6 or 7 units. As the A2 phase decomposes it breaks up into small (2 x 3) islands of face sharing hexagon rows, separated by regularly spaced defects. These defects can often be recognized as fragments of the A1 chain structure, as, for example, in Fig. 3c, lower left where the P type chain appears between two (2 x 3) domains. The structure between the hexagonal rows is indistinct and appears variable, with evidence for both pairs of small ring and larger voids between the rows, then what appears to be an empty channel to the next domain, as illustrated in Fig. 6a.

Understanding the structure of the 2D phase on Ni(110) is complicated both by its variability and uncertainty over its composition. The appearance of the short hexagonal face sharing chains above 150 K is clearly associated with the onset of dissociation to form OH, but it is not clear if

dissociation ceases with completion of the (2 x 3) structure or continues while there is intact water on the surface. The slight differences between the shape and width of the A2 desorption peak, which is smaller and wider for D_2O than for H_2O at low coverage, point to slightly different rates of dissociation for the two isotopes during desorption (either due to the higher tunneling rate of H versus D or to the larger H_2O zero point vibrational energy), initially changing the amount of OH(OD) present to stabilize the un-dissociated water. The evolution of the A2 phase between 180 and 220 K (see Figs. 2 & 3), where the (2 x 3) order persists, suggests that the overall OH/H_2O composition continues to change in this region and contributes to the changes in structure. Although XPS measurements by Pirug *et al.* found a 1:1 mixture of OH and H_2O [9] for this phase at 180 K, we can confidently assign this stoichiometry to the 1D chains of the A1 phase, present above 220 K, implying the A2 structure contains more water. On Cu(110), where the stoichiometry can be determined directly, the A2 structure has a (1OH : 2H_2O) composition and forms an ordered c(2x2) structure, consisting of a flat 2D network of distorted hexagonal face sharing rings. This structure is stabilized by the formation of strong H-bonds between water and OH, with OH arranged as dimers in Bjerrum defects [22]. The lateral density of water in this structure is 4.3% smaller than in the buckled hexagonal [0001] plane of bulk ice I_h, allowing the network to accommodate the O-O H-bond spacing and still bind water flat, bonded to Cu. Although the A2 structure formed on Ni also shows rows of hexagonal rings, these are interrupted by regular defects along the close packed direction, while the face sharing hexagonal rows do not appear next to each other in a c(2 x 2) arrangement but are spaced apart by an additional row along $[001]$. Ni has a 2.5% smaller lattice spacing than Cu, so the distorted hexagonal c(2 x 2) structure proposed earlier [9] would require a greater water density than in the buckled ice film. A surface repeat shorter than the usual O-O H-bond separation has previously been shown to result in disorder and strain relief in water films on Ru [49-50]. DFT calculations show an intact, c(2 x 2) water network would be highly buckled and energetically unfavorable [19], while formation of a flat c(2 x 2) OH-H_2O network would require a considerable lateral compression. The STM results presented here show the A2 structure on Ni(110) consists of short face sharing hexagonal rows periodically interrupted to relieve strain along $[1\bar{1}0]$, causing the ca. 6 unit LEED splitting observed, with the complete hexagonal c(2 x 2) structure modified in favor of more widely spaced (2 x 3) hexagonal rows.

Despite the disorder present in the A2 structure, and its uncertain OH/H_2O composition, it is useful to consider how OH stabilizes this 2D structure. Based on the 1:1 composition found by XPS, Pirug *et al.* originally suggested a c(2 x 2) distorted hexagonal network with alternating OH and H_2O groups completing the H-bond network [9]. This arrangement is similar to the flat OH-

H_2O phase found on hexagonal surfaces, including Pt(111) [51-54] and Pd(111) [55], and quite different to the D-type OH Bjerrum defects present in the structure found on Cu(110) [22]. In this case the structure sacrifices (weak) hydroxyl H-bonds to water in favor of maximizing the number of strong water H-bonds to hydroxyl. The short hexagonal rows formed on Ni(110) often show bright features along the row, for example in Fig. 6a, with the structure between the hexagonal rows showing lower contrast. These results suggest the network is corrugated, with the hexagonal rows being somehow different from the intermediate structure and containing some particular, periodic H-bond structures. On Cu(110) the OH Bjerrum defects that stabilize the water network image brighter than flat water in STM [22], suggesting the hexagonal bright features in the hexagonal rows on Ni(110) may also be Bjerrum defects stabilizing short hexagonal water rows. Although the Ni sites between the pairs of hexagonal rows also offer favorable binding sites for water, it is not possible to arrange a complete monolayer without suffering the lateral strain described earlier. Figure 6b suggests possible arrangements of water in this region, to create face sharing pentamers or octamer rings that broadly mimic the different sized rings observed. Ordered structures containing alternating face sharing pentamer and octamer rings, sandwiched between extended hexagonal water rows, have been found in the first layer of water on Cu(511) [43] and as a strain relief structure in second layer water on Pt and Ru [49, 56]. However, the lack of long range order in the structure between the hexagonal rows on Ni(110) makes it difficult to determine exactly what encourages their 3x ordering. What is clear is that this structure is neither the simple c(2 x 2) hexagonal Bjerrum defect network found on Cu(110) [22], nor the previously proposed flat c(2 x 2) OH-H_2O network [9].

Conclusion

Water dissociates spontaneously on Ni(110) as the surface is heated from 150 to 180 K, stabilizing water into short, face sharing hexagonal rows within a disordered (2 x 3) structure. The 2D network is interrupted by regular strain relief features that bisect the water/hydroxyl network in both directions, allowing the structure to accommodate the longer O-O spacing within the hexagonal rows to the short Ni-Ni spacing of the template. This structure accommodates a range of water/OH composition, possibly by forming OH Bjerrum defects, with disordered, variable structure between the hexagonal rows. The 2D network decomposes above 220 K to form a (OH-H_2O) phase, consisting of zizgzag water chains, stabilized by donation to OH. The (OH-H_2O) chains repel each other, ordering into a (2 0, 1 4) structure that decomposes to OH near 245 K as further water desorbs.

Supporting Information. LEED data and schematic showing surface repeat as a function of the anneal temperature.

Acknowledgements

This work was supported by the EPSRC via grants EP/K039687/1 and SCG10020.

References

1. Wang, D.; Astruc, D., The recent development of efficient Earth-abundant transition-metal nanocatalysts. *Chem. Soc. Rev.* **2017,** *46*, 816-854.

2. Aziz, M. A. A.; Jalil, A. A.; Triwahyono, S.; Ahmad, A., CO2 methanation over heterogeneous catalysts: recent progress and future prospects. *Green Chem.* **2015,** *17*, 2647-2663.

3. De, S.; Zhang, J. G.; Luque, R.; Yan, N., Ni-based bimetallic heterogeneous catalysts for energy and environmental applications. *Energy Environ. Sci.* **2016,** *9*, 3314-3347.

4. Pistonesi, C.; Juan, A.; Irigoyen, B.; Amadeo, N., Theoretical and experimental study of methane steam reforming reactions over nickel catalyst. *A. Surf. Sci.* **2007,** *253*, 4427-4437.

5. Mohsenzadeh, A.; Richards, T.; Bolton, K., DFT study of the water gas shift reaction on Ni(111), Ni(100) and Ni(110) surfaces. *Surf. Sci.* **2016,** *644*, 53-63.

6. Gallagher, M.; Omer, A.; Haq, S.; Hodgson, A., Water monolayer and multilayer adsorption on Ni(111). *Surf. Sci.* **2007,** *601*, 268-273.

7. Shiotari, A.; Sugimoto, Y.; Kamio, H., Characterization of two- and one-dimensional water networks on Ni(111) via atomic force microscopy. *Phys. Rev. Mat.* **2019,** *3*, 093001.

8. Michaelides, A.; Morgenstern, K., Ice nanoclusters at hydrophobic metal surfaces. *Nat. Mat.* **2007,** *6*, 597-601.

9. Pirug, G.; Knauff, O.; Bonzel, H. P., Structural and chemical aspects of H2O adsorption on Ni(110). *Surf. Sci.* **1994,** *321*, 58-70.

10. Andersson, K.; Ketteler, G.; Bluhm, H.; Yamamoto, S.; Ogasawara, H.; Pettersson, L. G. M.; Salmeron, M.; Nilsson, A., Autocatalytic water dissociation on Cu(110) at near ambient conditions. *J. Am. Chem. Soc.* **2008,** *130*, 2793-2797.

11. Mohsenzadeh, A.; Bolton, K.; Richards, T., DFT study of the adsorption and dissociation of water on Ni(111), Ni(110) and Ni(100) surfaces. *Surf. Sci.* **2014,** *627*, 1-10.

12. Seenivasan, H.; Tiwari, A. K., Water adsorption and dissociation on Ni(110): How is it different from its close packed counterparts? *J. Chem. Phys.* **2014,** *140*, 174704.

13. Zhu, L.; Liu, C. L.; Wen, X. D.; Li, Y. W.; Jiao, H. J., Coverage dependent structure and energy of water dissociative adsorption on clean and O-pre-covered Ni(100) and Ni(110). *Catal. Sci. Technol.* **2019,** *9*, 4725-4743.

14. Bange, K.; Grider, D. E.; Madey, T. E.; Sass, J. K., The surface chemistry of H2O on clean and oxygen covered Cu(110). *Surf. Sci.* **1984,** *136*, 38-64.
15. Nobl, C.; Benndorf, C.; Madey, T. E., H2O adsorption on Ni(110) - evidence for oriented water dimers. *Surf. Sci.* **1985,** *157*, 29-42.
16. Benndorf, C.; Madey, T. E., Adsorption of H2O on clean and oxygen-predosed Ni(110). *Surf. Sci.* **1988,** *194*, 63-91.
17. Schiros, T.; Haq, S.; Ogasawara, H.; Takahashi, O.; Öström, H.; Andersson, K.; Pettersson, L. G. M.; Hodgson, A.; Nilsson, A., Structure of water adsorbed on the open Cu(110) surface: H-up, H-down, or both? *Chem. Phys. Lett.* **2006,** *429*, 415-419.
18. Carrasco, J.; Michaelides, A.; Forster, M.; Raval, R.; Hodgson, A., A novel one dimensional ice structure built from pentagons. *Nat. Mat.* **2009,** *8*, 427-431.
19. Gerrard, N.; Mistry, K.; Darling, G. R.; Hodgson, A., Formation of linear water chains on Ni(110). *J. Phys. Chem. Lett.* **2020,** *11*, 2121-2126.
20. Spitzer, A.; Luth, H., An XPS study of the water-adsorption on Cu(110). *Surf. Sci.* **1985,** *160*, 353-361.
21. Pang, Z. Q.; Duerrbeck, S.; Kha, C.; Bertel, E.; Somorjai, G. A.; Salmeron, M., Adsorption and reactions of water on oxygen-precovered Cu(110). *J. Phys. Chem. C* **2016,** *120*, 9218-9222.
22. Forster, M.; Raval, R.; Hodgson, A.; Carrasco, J.; Michaelides, A., c(2 x 2) water-hydroxyl layer on Cu(110): a wetting layer stabilized by Bjerrum defects. *Phys. Rev. Lett.* **2011,** *106*, 046103.
23. Guo, H. S.; Zaera, F., Reactivity of hydroxyl species from coadsorption of oxygen and water on Ni(110) single-crystal surfaces. *Catalysis Letters* **2003,** *88*, 95-104.
24. Benndorf, C.; Nobl, C.; Madey, T. E., H2O adsorption on oxygen-dosed Ni(110) - formation and orientation of OH(ad). *Surf. Sci.* **1984,** *138*, 292-304.
25. Olle, L.; Salmeron, M.; Baro, A. M., The adsorption and decomposition of water on Ni(110) studied by electron-energy loss spectroscopy. *J. Vac. Sci. Techn. A* **1985,** *3*, 1866-1870.
26. Hock, M.; Seip, U.; Bassignana, I.; Wagemann, K.; Kuppers, J., Coadsorption of oxygen and water at Ni(110) surfaces. *Surf. Sci.* **1986,** *177*, L978-L982.
27. Callen, B. W.; Griffiths, K.; Memmert, U.; Harrington, D. A.; Bushby, S. J.; Norton, P. R., The adsorption of water on Ni(110) - monolayer, bilayer and related phenomena. *Surf. Sci.* **1990,** *230*, 159-174.
28. Callen, B. W.; Griffiths, K.; Norton, P. R., Reorientation of chemisorbed water on Ni(110) by hydrogen-bonding to 2nd-layer. *Phys. Rev. Lett.* **1991,** *66*, 1634-1637.

29. Callen, B. W.; Griffiths, K.; Kasza, R. V.; Jensen, M. B.; Thiel, P. A.; Norton, P. R., Structural phenomena related to associative and dissociative adsorption of water on Ni(110). *J. Chem. Phys.* **1992,** *97*, 3760-3774.

30. Callen, B. W.; Griffiths, K.; Norton, P. R., Observation of free hydroxyl-groups on the surface of ultra thin ice layers on Ni(110). *Surf. Sci.* **1992,** *261*, L44-L48.

31. Callen, B. W.; Griffiths, K.; Norton, P. R.; Harrington, D. A., Autocatalytic decomposition of water on Ni(110). *J. Phys. Chem.* **1992,** *96*, 10905-10913.

32. Pangher, N.; Schmalz, A.; Haase, J., Structure determination of water chemisorbed on Ni(110) by use of X-ray-absorption fine-structure measurements. *Chem. Phys. Lett.* **1994,** *221*, 189-193.

33. Forster, M.; Raval, R.; Carrasco, J.; Michaelides, A.; Hodgson, A., Water-hydroxyl phases on an open metal surface: breaking the ice rules. *Chem. Sci.* **2012,** *3*, 93-102.

34. Winkler, A.; Rendulic, K. D., Adsorption-kinetics for hydrogen adsorption on nickel and coadsorption of hydrogen and oxygen. *Surf. Sci.* **1982,** *118*, 19-31.

35. Christmann, K.; Chehab, F.; Penka, V.; Ertl, G., Surface reconstruction and surface explosion phenomena in the nickel (110) hydrogen system. *Surf. Sci.* **1985,** *152*, 356-366.

36. McBride, F.; Hodgson, A., Water and its partially dissociated fragments at metal surfaces. *Int. Rev. Phys. Chem.* **2017,** *36*, 1-38.

37. Guo, H. S.; Zaera, F., The reactivity of hydroxyl groups toward ammonia on Ni(110) surfaces. *Surf. Sci.* **2003,** *524*, 1-14.

38. Zhao, W.; Bajdich, M.; Carey, S.; Vojvodic, A.; Norskov, J. K.; Campbell, C. T., Water Dissociative adsorption on NiO(111): energetics and structure of the hydroxylated surface. *ACS Catal.* **2016,** *6*, 7377-7384.

39. Yuzawa, T.; Higashi, T.; Kubota, J.; Kondo, J. N.; Domen, K.; Hirose, C., CO coadsorption-induced recombination of surface hydroxyls to water on Ni(110) surface by IRAS and TPD. *Surf. Sci.* **1995,** *325*, 223-229.

40. Seh, Z. W.; Kibsgaard, J.; Dickens, C. F.; Chorkendorff, I. B.; Norskov, J. K.; Jaramillo, T. F., Combining theory and experiment in electrocatalysis: insights into materials design. *Science* **2017,** *355,* eaad4998.

41. Tsai, C.; Lee, K.; Yoo, J. S.; Liu, X. Y.; Aljama, H.; Chen, L. D.; Dickens, C. F.; Geisler, T. S.; Guido, C. J.; Joseph, T. M.; *et al.*, Direct water decomposition on transition metal surfaces: structural dependence and catalytic screening. *Catal. Lett.* **2016,** *146*, 718-724.

42. Bertram, C.; Auburger, P.; Bockstedte, M.; Stabler, J.; Bovensiepen, U.; Morgenstern, K., Impact of Electron Solvation on Ice Structures at the Molecular Scale. *J. Phys. Chem. Lett.* **2020,** *11*, 1310-1316.

43. Lin, C.; Avidor, N.; Corem, G.; Godsi, O.; Alexandrowicz, G.; Darling, G. R.; Hodgson, A., Two-dimensional wetting of a stepped copper surface. *Phys. Rev. Lett.* **2018,** *120*, 076101.

44. Horcas, I.; Fernandez, R.; Gomez-Rodriguez, J. M.; Colchero, J.; Gomez-Herrero, J.; Baro, A. M., WSXM: A software for scanning probe microscopy and a tool for nanotechnology. *Rev. Sci. Instrum.* **2007,** *78*, 013705.

45. Thiel, P. A.; Madey, T. E., The interaction of water with solid surfaces: fundamental aspects. *Surf. Sci. Rep.* **1987,** *7*, 211-385.

46. Roux, C. D.; Bu, H.; Rabalais, J. W., Structure of the Ni(110)-p(2 X 1)-OH surface from time-of-flight scattering and recoiling spectrometry. *Surf. Sci.* **1992,** *279*, 1-12.

47. Shi, Y.; Choi, B. Y.; Salmeron, M., Water chains guide the growth of monoatomic copper wires on Cu(110). *J. Phys. Chem. C* **2013,** *117*, 17119-17122.

48. Kumagai, T.; Kaizu, M.; Okuyama, H.; Hatta, S.; Aruga, T.; Hamada, I.; Morikawa, Y., Tunneling dynamics of a hydroxyl group adsorbed on Cu(110). *Phys. Rev. B* **2009,** *79*, 035423.

49. Maier, S.; Lechner, B. A. J.; Somorjai, G. A.; Salmeron, M., Growth and structure of the first layers of ice on Ru(0001) and Pt(111). *J. Am. Chem. Soc.* **2016,** *138*, 3145-3151.

50. Gallagher, M.; Omer, A.; Darling, G. R.; Hodgson, A., Order and disorder in the wetting layer on Ru(0001). *Faraday Discuss. Chem. Soc.* **2009,** *141*, 231-249.

51. Michaelides, A.; Hu, P., A density functional theory study of hydroxyl and the intermediate in the water formation reaction on Pt. *J. Chem. Phys.* **2001,** *114*, 513-519.

52. Held, G.; Clay, C.; Barrett, S.; Haq, S.; Hodgson, A., Structure of mixed OH+H2O overlayers on Pt(111). *J. Chem. Phys.* **2005,** *123*, 064711.

53. Karlberg, G. S.; Wahnstrom, G., An interaction model for OH+H2O-mixed and pure H2O overlayers adsorbed on Pt(111). *J. Chem. Phys.* **2005,** *122*, 194705.

54. Schiros, T.; Ogasawara, H.; Naslund, L. A.; Andersson, K. J.; Ren, J.; Meng, S.; Karlberg, G. S.; Odelius, M.; Nilsson, A.; Pettersson, L. G. M., Cooperativity in surface bonding and hydrogen bonding of water and hydroxyl at metal surfaces. *J. Phys. Chem. C* **2010,** *114*, 10240-10248.

55. Clay, C.; Cummings, L.; Hodgson, A., Mixed water/OH structures on Pd(111). *Surf. Sci.* **2007,** *601*, 562-568.

56. Gerrard, N.; Gattinoni, C.; McBride, F.; Michaelides, A.; Hodgson, A., Strain relief during ice growth on a hexagonal template. *J. Am. Chem. Soc.* **2019,** *141*, 8599-8607.

TOC

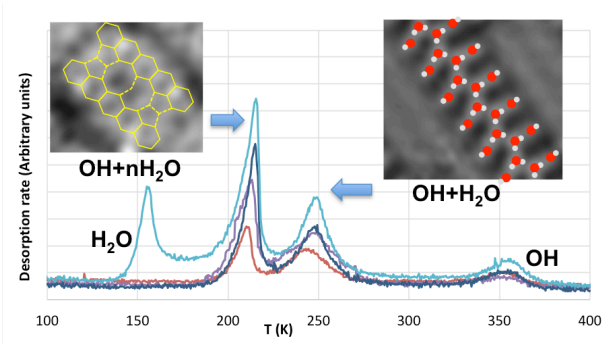
OH+nH2O
OH+H2O
H2O
OH
Desorption rate (Arbitrary units)
100
150
200
250
300
350
400
T (K)